SOURCE CHARACTERISTICS OF EVENTS IN THE SAN FRANCISCO BAY REGION

Award Number 1434-93-G2311

Program Element II, Component II

Douglas S. Dreger and Barbara Romanowicz (PI)

Seismographic Station, 475 McCone Hall
University of California, Berkeley, CA 94720

Telephone: (510)642-3977 Fax:(510)643-5811

Email: dreger@seismo.berkeley.edu barbara@seismo.berkeley.edu

Key words: Velocity models, moment tensors, finite faults

Research Supported by the U.S. Geological Survey (USGS), Department of the Interior, under USGS award number 1434-93-G2311. The views and conclusions contained in this document are those of the authors and should not be interpreted as necessarily representing the official policies, either expressed or implied, of the U.S. Government.

FILE COPY

Abstract

This report summarizes the main results obtained under award 1434-93-G2311 of the U.S. Geological Survey to study the source characteristics of earthquakes in the San Francisco Bay area and surrounding regions. The results of this study have been published in two Geophysical Research Letter articles (Romanowicz et al., 1993; Dreger et al., 1995). During the project period we have made several accomplishments. First, we have analyzed broadband waveforms of earthquakes occurring throughout central and northern California to calibrate the low-frequency, long-wavelength crustal structure. As described in the following section we have found that two one-dimensional models, one for the central Coast Ranges and the other for the Sierra Nevada and southern California, are sufficient for routine estimation of seismic moment tensors for events ranging in magnitude from M_w 3.5 to approximately 7.0. Second, a catalog of Green's functions has been computed for easy online access facilitating rapid moment tensor analysis and other earthquake source studies. Third, we have developed fully automated moment tensor routines which currently enable the estimation of moment tensors throughout the region within 9 to 15 minutes following an event (Pasyanos et al., 1995). Finally, we have written computer code which enables the estimation of finite source parameters using far-field moment rate functions derived from regional distance broadband waveforms. This work was done in conjunction with a study of the 1994 Northridge mainshock and aftershocks (Dreger, 1994) which was supported through NSF and NEHRP to investigate the Northridge sequence. We used this methodology to investigate the source process of the 1993 Klamath Falls sequence (Dreger et al., 1995) and other significant earthquakes.

Investigations Undertaken

Velocity Model Regionalization

We have found that two primary velocity model domains are required at long-periods to compute moment tensor solutions of earthquakes ranging in size from M_w 3.5 to approximately M_w 7.0. The velocity model domains are defined based on the similarity of near-surface velocities and crustal thickness of USGS models (Figure 1), the refraction results of Fuis and Mooney (1990), and by broadband waveform modeling. Figure 2 shows the boundaries of the two velocity model domains, a subset of M_w 4.0 and larger events we have analyzed since 1990, and the current configuration of the Berkeley Digital Seismic Network (BDSN).

Coast Ranges Domain. The Coast Ranges have an average crustal thickness of 25 km (Fuis and Mooney, 1990) with significant variation in surface velocity (Figure 1). Our initial efforts at developing a model for this domain focussed on the immediate surroundings of the San Francisco Bay area. Two paths were considered, namely the path from the Geysers and the path from Gilroy. These paths were chosen because data was recorded at several BDSN stations for the M_w 4.6 Geysers and M_w 4.9 Gilroy earthquakes (events 13 and 22, Figure 2). The distances of these two events to the BKS station are nearly the same (119 km compared to 117 km), but the paths traverse completely different regions, and provide the opportunity to directly compare the waveforms to identify differences in their characteristics and the implied differences in wave propagation.

The path from the Geysers traverses a heterogeneous stretch of the Coast Ranges consisting of Franciscan assemblage, Quaternary and Upper Tertiary Volcanic rocks, as well as Quaternary alluvium, and intertidal deposits. The final 20 to 30 km traversed the Quaternary basin deposits of the San Pablo Bay. Model MTM (Table 1) was developed for this

path using the broadband data (0.01 to 5.0 Hz) recorded at BKS and MHC. This model represents the upper bound of near-surface velocities represented by the USGS crustal models (Figure 1). On the other hand, the upper crust along the path from Gilroy is dominated by the Quaternary sediments of the San Francisco Bay area. Model GIL7 was developed for the path to MHC and BKS. The surface velocities are found to be much slower than those in model MTM, and represent a lower bound on the range of near-surface velocities of the USGS models (Figure 1).

Figure 3 compares the broadband (0.02 to 2.0 Hz), tangential component displacement data recorded at BKS for the Geysers and Gilroy earthquakes with synthetics computed with the MTM and GIL7 velocity models, respectively. Note that the Geysers waveform is simpler than the Gilroy waveform in that the duration of large motions is several tens of seconds shorter. The Gilroy path clearly produces a dispersed Love wave train while the Geysers path does not. This is reflected in the near surface velocity gradients of the two models. In terms of the body phases, the difference in relative timing of the SmS and sScS phases observed for the two events is due to differences in source depth, where the Geysers earthquake occurred at a depth of 2 km and the Gilroy earthquake ruptured at 7 km depth. The phase sScS is a depth phase which is reflected from an interface at approximately 16 to 17 km depth. Arrivals from this lower crustal interface have also been observed from reflection data obtained from the BASIX experiment (e.g. Brocher et al., 1994)

There is certainly room for refinement of the MTM model to better fit the higher frequency phases and the phase of the Love wave of the Geysers data, however at long-periods (0.01 to 0.1 Hz) this model is found to fit the three-component data quite well. At periods which are commonly used in moment tensor determinations at regional distances (e.g. Dreger and Helmberger, 1993; Ritsema and Lay, 1993; Walter, 1993) either model MTM or GIL7 is sufficient, because at periods longer than 10 s the waves are most sensitive to only the average crustal velocity and crustal thickness which are both approximately the same (Table 1). Figure 4 illustrates through the use of the cross-correlation function that the level of fit obtained for each of the models to the Gilroy data improves with decreasing frequency. The GIL7 model, however, clearly fits the Gilroy data better in a broadband sense.

We have also found that the GIL7 model explains P_{nl} and S_n waveforms of Cape Mendocino events recorded at regional distances as well as for events located to the south of the San Francisco Bay Area. Thus, the GIL7 model appears to have a wide area of applicability based on waveform modeling of additional source-station pairs, and through the comparison of the complete waveform derived moment tensor solutions with both those from first motions and regional surface wave amplitude and phase spectra (Pasyanos et al., 1995). The dashed lines on Figure 2 show the demarcation of the GIL7 domain which we now routinely use.

Sierra Nevada Domain. The Sierra Nevada domain in contrast to the central Coast Ranges is characterized by a thicker crust and faster near-surface velocities than the Coast Ranges (Table 1). The average crustal thickness is approximately 35 km, and the thickest region reaches 55 km (Fuis and Mooney, 1990), although a more recent tomographic and refraction study (Jones et al., 1994) suggests a more uniform 33 km crustal thickness beneath the southern Sierra Nevada. The velocities of surfical granitic rock of the Sierran Batholith are approximately 0.5 to 1 km/s faster than in the central Coast Ranges. The average crustal velocities are 0.3 km/s faster. Model SoCal (Table 1) which was derived from traveltime studies (Hadley and Kanamori, 1977), teleseismic Rayleigh wavs (Hadley and Kanamori, 1979), and broadband waveform modeling (Dreger and Helmberger, 1993; Dreger, 1992) is similar to the USGS AUB and WAL models (Figure 1).

Figure 5 compares three-component displacement data for a M_w 4.1 earthquake located near Quincy, CA. (event 57, Figure 2) recorded at the ORV station (distance of 71 km) with synthetics computed with the SoCal model. This model gives a very good level of fit to the three-component data. The tangential component waveforms are relatively simple compared to those for the Gilroy earthquake (Figure 6). Differences in wave propagation in the two velocity model domains can be clearly seen in Figure 6 in which the tangential displacement records of the Gilroy earthquake recorded at BKS (distance of 117 km) are compared to those of an aftershock of event 38 (Figure 2) recorded at CMB (distance of 106 km). These two seismograms, although observed at nearly the same distances, show significant differences in the character of both body and surface wave development.

Regional Moment Tensor Analysis

To date we have analyzed 127 moment tensors of events ranging in size from M_w 3.5 to 7.0 using the velocity model regionalization scheme described above. During this time period the moment tensor solutions reveal the heterogeneous style of faulting occurring throughout the northern two-thirds of the state of California. The San Andreas system is represented by right-lateral strike-slip mechanisms. Event 44 (Figure 2) is a M_w 5.0 earthquake which occurred adjacent to the Parkfield nucleation zone on December 20, 1994. Both west and east of the San Andreas fault in central California events 3, 21 55 and 56 (Figure 2) have thrust mechanisms. Events 21, 55, 56 have a San Andreas fault normal compressive stress axis orientation which is consistent with the observations of Zoback et al. (1987). The western Basin and Range province extending into eastern California is marked by both normal and strike-slip mechanisms. In this region there are east-west to northwest-southeast oriented tensional stress axes. Two major sequences have occurred during this period namely, the May 17, 1993 M_w 6.1 Eureka Valley (events 18, 19, 20 Figure 2) and the September 12, 1994 M_w 6.0 Double Springs Flat (events 38, 39 Figure 2). We are currently writing a journal article discussing the source characteristics of these sequences.

On September 21, 1993 a sequence of two M_w 6.0 mainshocks and 10 aftershocks with magnitudes greater than 4.0 occurred in southern Oregon. These were normal-slip events with southwest-northeast striking tension axes. We performed a detailed analysis of moment tensor solutions of the 20 largest earthquakes in the sequence as well as the rupture history of the two mainshocks which was reported on in Geophysical Research Letters (Dreger et al., 1995) and is included in the appendix of this report for reference.

The Mendocino Triple Junction was the most active region of northern California. Five M_w 6 and larger earthquakes occurred during this period namely the 1992 Petrolia earthquake and aftershocks (events 6,7 and 8 Figure 2), an event along the Mendocino Transform fault (event 37 Figure 2) and another within the Gorda Plate (event 47 Figure 2). In addition, a shallow earthquake displaying extensional tectonics occurred within the North American Plate (event 58 Figure 2). A nearby earthquake (event 59 Figure 2) occurred at a depth of 40 km and reveals the general north-south compressive stress regime observed in the Gorda plate for offshore events persists in the subducted Gorda plate.

Automated Moment Tensor Estimation

We have automated the moment tensor procedures to facilitate routine determinations as well as to improve rapid analysis. The time domain moment tensor procedure is activated using the UNIX *cron* function which reads the system mailbox every 3 minutes to search for

event messages issued by the Rapid Data Integration System (REDI) (Gee et al., 1995). If a message is found for an event with a preliminary magnitude of 3.5 or greater a working directory is created, the waveform data is extracted from the Northern California Earthquake Data Center, the data is rotated and filtered and then inverted using Green's functions stored in an online catalog.

Currently, the minimum magnitude which is processed is set at M3.5. This value reflects the limits imposed by the background noise in the frequency passband used by the inversion. Three passbands are employed: 50 to 10 seconds ($3.5 \geq M < 4.0$), 50 to 20 seconds ($4.0 < M < 5.0$), and 100 to 20 seconds ($M \geq 5.0$). The two velocity models described in the last section are used, however to obtain the desired reduction in moment tensor processing time the theoretical Green's functions computed using these models are stored online. These Green's functions are prefiltered using the three passbands described above.

The inverse procedure itself makes several assumptions. First, it is constrained to only the deviatoric tensor neglecting volumetric changes of the source. Second, a point-source is assumed. Source depth is found by iteration and evaluating an objective function which depends upon both the RMS of the difference between the data and the synthetic waveforms, modulated by the percent double couple (pdc):

$$fit = \frac{RMS(data - synth)}{pdc} \tag{1}$$

Smaller numbers indicating better fits are obtained when both the difference of the waveforms is small and the pdc is large. Another measure which is used is the variance reduction:

$$1.0 - \frac{\int [d - s]^2 dt}{\int d^2 dt} \tag{2}$$

where d is the data and s is the synthetic.

The current procedure utilizes the three closest stations in the distance range from 50 to 400 km. This ensures reasonably good azimuthal coverage. Although the inversion of complete three-component waveform data from a single station may resolve the moment tensor parameters (Dreger and Helmberger, 1991) the use of multiple stations improves the stability of the results (Dreger and Helmberger, 1993). Figure 7 demonstrates the automated moment tensor method for a small earthquake and compares the results with a final analyst reviewed solution. In this particular case, the 50 to 20 second passband was used. The revised solution, which was released via email, was obtained by searching the depth parameter space (the depth remained at 11 km), and adding station CMB to provide better azimuthal coverage, particularly by adding P_{nl} and Rayleigh waves. Clearly the automated and revised solutions are nearly the same, and in this particular case processing was completed 9 minutes from the origin time.

Since November 1993 we have been disseminating the preliminary moment tensor results via email and have been archiving them online. To ensure the robustness of the information we release and to provide redundancy in the automated system we also run a surface wave amplitude and phase spectral inversion in parallel (Romanowicz, et al., 1993; Pasyanos et al., 1995).

Regional Distance Finite Fault Estimation

To resolve the fault plane ambiguity inherent in the moment tensor analysis given the point-source assumption, and also to estimate directivity and slip distribution for the larger events we have developed an empirical Green's function (EGF) deconvolution approach which can be applied to regional distance broadband data. The wide dynamic range of the BDSN records the full spectrum of wave motions from the smallest to largest events onscale. The recorded ground motions due to earthquakes are essentially the radiated wavefield with a number of filters applied, where,

$$U(\omega) = S(\omega) * G(\omega) * I(\omega). \tag{3}$$

$U(\omega)$ is the displacement spectrum recorded at the station, $S(\omega)$ is the source spectrum, $G(\omega)$ is the Green's function spectrum which represents the interaction of waves with the earth's structure including local site effects and attenuation properties and $I(\omega)$ is the instrument transfer function. By deconvolving the shared $G(\omega)$ and $I(\omega)$ terms of a nearly collocated aftershock or other earthquake with similar focal mechanism and a source dimension much smaller than that of the mainshock the ratio of the displacement spectra may be written as

$$\frac{U(\omega)_{main}}{U(\omega)_{egf}} = S(\omega)_{main}. \tag{4}$$

Equation (4) assumes that the source spectrum of the EGF is white in the limited band where the deconvolution is performed.

In practice the three component data are deconvolved independently using the frequency domain approach described above with the addition of a "water level" (Clayton and Wiggins, 1976) applied to the EGF spectra to fill spectral holes which can lead to deconvolution instability. The water level is usually chosen to be between only 1 to 5% of the peak spectral level of the EGF to not severely modify the original spectra. The three-component deconvolutions are then stacked to reduce noise levels. As an example of the deconvolution procedure, Figure 8 compares the stacked three-component deconvolutions at the VTV station for the 1994 Northridge earthquake (see reprint in the appendix). The EGF waveform is very complicated, particularly at short-periods, and it would be very challenging to develop a suitable theoretical Green's function for this path to model higher frequencies. The stacked three-component deconvolutions yield a well resolved far-field moment rate function (MRF) however. Thus, this approach is particularly attractive in uncalibrated regions and in areas where complex earth structure severely modifies the regional waveforms.

Ideally, the deconvolutions would be performed on specific phases and the station-subfault timing would be handled using ray tracing through a reasonable velocity structure (e.g. Mori and Hartzell, 1990; Antolik et al., 1995). At regional distances, however, it is not possible to isolate individual phases in the complex waveforms and a half-space ray trajectory is used. An analysis of the entire procedure using synthetic seismograms revealed that the half-space ray trajectory assumption is reasonable at regional distances, and that the method is capable of recovering the locations of high slip regions on the fault plane.

Inversion Method. The inversion method is described in detail in Mori and Hartzell (1990) and Dreger (1994) and will be briefly outlined in this context. Essentially the inverse procedure makes the assumption that MRF shape may be mapped into the spatial and temporal distribution of fault slip, and constitutes a perturbation to the point-source approximation implied by the deconvolution process. The rupture model consists of a radial rupture front

propagating at constant velocity with slip distributed across the plane. The method allows resolution of multi-dimensional rupture directivity constrained to a plane. The fault model is discretized into many subfaults and the slip at each is determined by the inversion of the following system of equations,

$$D_i(t) = MRF(t) = \sum_{j}^{m} \frac{\mu A u_j}{M_0} B_j(t - \tau_{ij}) \tag{5}$$

$$\left[\frac{B}{\lambda \frac{du}{da}}\right] u = \left[\frac{D}{0}\right]. \tag{6}$$

B is the radiated source function which is delayed by τ_{ij} which is a function of both the radial rupture front arrival time and the relative subfault-station distance. For simplicity B is defined as a constant width boxcar function. The MRF are the far-field moment rate functions and are the observed data. μ, A, u_j, and M_0 are the rigidity, the subfault area, the subfault slip and the scalar seismic moment of the mainshock, respectively. The indices i and j refer to the stations and subfaults respectively, and m is the total number of subfaults. M_0 is obtained independently from the moment tensor inversion of long-period waveforms. $\frac{du}{da}$ is a first spatial derivative smoothing constraint added for stability, and λ weights the smoothing function. The system of equations is solved using non-negative least squares (Lawson and Hanson, 1974) to consider only unidirectional slip.

Inversion Results. We have applied this technique to a number of recent moderate to large earthquakes, namely, M_w 6.1 Joshua Tree, CA (Hough and Dreger, 1995), two M_w 6.0 Klamath Falls, OR events (Dreger et al., 1993), M_w 6.7 Northridge, CA (Dreger, 1994), and the M_w 5.0 Parkfield, CA event. Reprints of papers describing the Klamath Falls, OR and Northridge, CA events are included in the appendix. The Parkfield earthquake serves as a useful example illustrating the technique.

Figure 9 shows the location of the Parkfield event and the four closest broadband stations from BDSN (CMB and MHC) and TERRAscope (SBC and ISA). The moment tensor solution was obtained by inverting long-period complete waveforms at these stations. The seismic moment was found to be $3.2x10^{23}$ dyne cm, and the centroid depth is 8 km. Figure 9b shows three component stacked moment rate functions obtained by deconvolving the seismograms of a smaller M_w 4.4 event which occurred on October 20, 1992. The stacked moment rate functions reveal shorter duration pulses at stations to the north indicating a component of directivity in that direction, however over all, the durations are similar indicating that the rupture expanded in a manner more complex then simply unilaterally to the northwest. Figure 10 shows the slip map obtained by inverting the moment rate functions. Curiously, this event ruptured a section of fault which had been previously aseismic and does not overlap with areas that ruptured during three earlier M_w 4.4, 4.4, 4.8 events (Johnson et al., 1995). This event occurred adjacent to the Middle Mountain nucleation zone of the 1934 and 1966 Parkfield earthquakes (distance 0 on Figure 10) in an area where the rupture of the next Parkfield earthquake is expected to rupture. The peak slip, however, is very low for the area required by the moment rate functions indicating that this event is very low stress drop. We estimated a stress drop of 3 bars which is consistent with those obtained from local acceleration data (Hellweg et al., 1995), and regional coda envelopes (Mayeda and Walter, 1995), and suggests that this event may only represent partial stress drop in the region adjacent to the Parkfield nucleation zone.

Conclusions

In conclusion, we have calibrated the low-frequency, long-wavelength velocity structure of central and northern California. We have found that the use of two velocity models is adequate for the routine estimation of seismic moment tensors throughout the region. The moment tensor code has been fully automated facilitating routine analysis and rapid response. Currently we are able to obtain preliminary moment tensor solutions for M_w 3.5 to 7.0 earthquakes within the REDI processing region (Gee et al., 1995) within 9 to 15 minutes after the origin time. The lower threshold of processable earthquakes is due to the back ground noise levels in the frequency pass bands that are used. The upper limit is determined by the breakdown of the point-source assumption for the largest events.

We have developed a method of extracting finite fault information from relatively sparse regional broadband network data. In this approach we remove the influences of crustal structure on the waveforms by using the empirical Green's function approach. The resulting far-field moment rate functions are then inverted for the position and timing of slip distributed on one of the two possible nodal planes. This approach has been shown to be effective in the resolution of the fault plane ambiguity (Mori and Hartzell, 1990), the estimation of stress drop taking into account multidimensional source directivity (e.g. Hough and Dreger, 1995), and in estimating the character of distributed slip for a class of earthquakes which would ordinarily escape such scrutiny because of the lack of availability of data from dense local networks of strong motion instrumentation. Furthermore the rapid telemetry afforded by BDSN coupled with rapid moment tensor estimation to identify potential empirical Green's functions allows rapid finite fault analysis which potentially can be obtained in a time frame useful for post earthquake emergency response.

Reports Published

Dreger, D., J. Ritsema, and M. Pasyanos, Broadband Analysis of the 21 September, 1993, Klamath Falls Sequence, *Geophys. Res. Lett.,* 22, 997-1000, 1995.

Romanowicz, B., D. Dreger, M. Pasyanos, and R. Uhrhammer, Monitoring of Strain Release in Central and Northern California Using Broadband Data, *Geophys. Res. Lett., 20,* 1643-1646, 1993.

References

Antolik, M., D. Dreger, and B. Romanowicz, Rupture Process of the March 9, 1994 Deep Fiji Islands Earthquake using an Empirical Green's Function Method, *submitted to J. Geophys. Res.,* 1995.

Brocher, T.M., J. McCarthy, P.E. Hart, W.S. Holbrook, K.P. Furlong, T. McEvilly, J.A. Hole, and S.L. Klemperer, Seismic Evidence for a Lower-Crustal Detachment Beneath San Francisco Bay, California, *Science,* 265, 1436-1439, 1994.

Clayton, R. W., and R. A. Wiggins, Source Shape Estimation and Deconvolution of Teleseismic Body Waves, *Geophys. J. R. Astron. Soc., 47,* 151-177, 1976.

Dreger, D. S., and D. V. Helmberger, Complex Faulting Deduced from Broadband Modeling of the 28 February 1990 Upland Earthquake (M_L=5.2), *Bull. Seism. Soc. Am.,* **81** 1129-1144, 1991.

Dreger, D. S., Modeling Local and Regional Distance Earthquakes with Broadband Data, Ph. D. thesis, Caltech, 1992.

Dreger, D. S. and D. V. Helmberger, Determination of Source Parameters at Regional Distances with Single Station or Sparse Network Data, *J. Geophys. Res., 98,* 8107-8125, 1993.

Dreger, D., Empirical Green's Function Study of the January 17, 1994 Northridge, California Earthquake, *Geophys. Res. Lett., 21,* 2633-2636, 1994.

Dreger, D., J. Ritsema, and M. Pasyanos, Broadband Analysis of the 21 September, 1993, Klamath Falls Sequence, *Geophys. Res. Lett.,* 22, 997-1000, 1995.

Fuis, G. S. and W. D. Mooney, Lithospheric Structure and Tectonics from Seismic Refraction and other Data, *U.S. Geol. Sur. Prof. Paper 1515,*207 - 236, 1990.

Gee, L. S., D. S. Neuhauser, D. Dreger, M. Pasyanos, R. A. Uhrhammer, and B. Romanowicz, Real-time Seismology Seismology at UC Berkeley: The Rapid Earthquake Data Integration Project, *submitted to Bull. Seism. Soc. Am.,* 1995.

Hadley, D. and H. Kanamori, Seismic Structure of the Transverse Ranges, *Bull. Seism. Soc. Am.,* 88, 1469-1478, 1977.

Hadley, D. and H. Kanamori, Regional S-wave Structure for Southern California from the Analysis of Teleseismic Rayleigh Waves, *Geophys. J. R. Intern.,* 58, 655-666, 1979.

Hellweg, M., J. Boatwright, J. B. Fletcher, C. Dietel, P. Spudich, L. Baker, and R. Borcherdt, Two Moderate Earthquakes at Parkfield, CA: November 14, 1993 and December 20, 1994, *Seism. Res. Let.,* 66, p 35, 1995.

Hough, S. E., and D. S. Dreger, Source Parameters of the 4/23/92 M6.1 Joshua Tree, California Earthquake and its Aftershocks: Empirical Green's Function Analysis of GEOS and TERRAscope Data, *in press Bull. Seism. Soc. Am.,* 1995.

Johnson, P. A., D. Dreger, and T. V. McEvilly, Source Characteristics of the Three Recent M4.7-5.0 Sequences in the Parkfield Nucleation Zone, *Seism. Res. Let.,* 66, p 36, 1995.

Jones, C., H. Kanamori, S. Roecker, W. Steven, Missing Roots and Mantle Drips: Regional Pn and Teleseismic Arrival Times in the Southern Sierra Nevada and Vicinity California, *J. Geophys. Res.,* 99, 4567-4601, 1994.

Lawson, C. L., and R. J. Hanson, Solving Least Squares Problems, Prentice-Hall, Inc., New Jersey, 1974.

Mayeda, K. and W. R. Walter, Source Parameters of Western U.S. Earthquakes: Moment, Energy, Stress Drop, and Source Spectra from Regional Coda Envelopes, *submitted to J. Geophys. Res.,* 1995.

Mori, J., and S. Hartzell, Source Inversion of the 1988 Upland Earthquake: Determination of a Fault Plane for a Small Event, *Bull. Seism. Soc. Am., 80,* 507-518, 1990.

Pasyanos, M. E., D. S. Dreger and B. Romanowicz, Towards Real-Time Determination of Regional Moment Tensors, *submitted to Bull. Seism. Soc. Am.,* 1995.

Ritsema, J., and T. Lay, Rapid Source Mechanism Determination of Large ($M_w >= 5$) Earthquakes in the Western United States, *Geophys. Res. Lett.,* 20, 1611-1614, 1993.

Romanowicz, B., D. Dreger, M. Pasyanos, and R. Uhrhammer, Monitoring of Strain Release in Central and Northern California Using Broadband Data, *Geophys. Res. Lett., 20,* 1643-1646, 1993.

Walter, W. R., Source Parameters of the June 29, 1992 Little Skull Mountain Earthquake from Complete Regional Waveforms at a Single Station, *Geophys. Res. Lett.,* 20, 403-406, 1993.

Zoback, M. D., M. L. Zoback, V. Mount, J. Eaton, J. Healy, D. Oppenheimer, P. Reasenburg, L. Jones, B. Raleigh, I. Wong, O. Scotti, and C. Wentworth, New Evidence on the State of Stress on the San Andreas Fault System, *Science,* 238, 1105-1111, 1987.

TABLE 1. Velocity Models

SoCal				GIL7				HAY				MTM			
α	β	ρ	Z	α	β	ρ	Z	α	β	ρ	Z	α	β	ρ	Z
5.50	3.18	2.40	0.0	3.20	1.50	2.28	0.0	3.77	2.18	2.28	0.0	4.50	2.60	2.28	0.0
6.30	3.64	2.67	5.5	4.50	2.40	2.28	1.0	4.64	2.68	2.28	1.0	4.80	2.76	2.58	3.0
6.70	3.87	2.80	16.0	4.80	2.78	2.58	3.0	5.34	3.08	2.67	3.0	5.51	3.18	2.68	6.0
7.80	4.50	3.30	35.0	5.51	3.18	2.58	4.0	5.75	3.32	2.67	6.0	5.95	3.44	2.79	12.0
				6.21	3.40	2.68	5.0	6.00	3.46	2.67	9.0	6.78	3.91	3.00	18.0
				6.89	3.98	3.00	17.0	6.22	3.59	2.80	14.0	7.83	4.52	3.26	27.0
				7.83	4.52	3.26	25.0	7.98	4.61	3.30	25.0				
Ave. crustal velocity = 3.69				Ave. crustal velocity = 3.39				Ave. crustal velocity = 3.34				Ave. crustal velocity = 3.37			

α and β are the P- and S-wave velocities in km/s and ρ is denisity in g/cc. Z is the depth to the top of the interface. The S-wave velocities for model HAY were computed assuming Poisson's rationship where $\alpha = \sqrt{3}\beta$. The layer thickness weighted average crustal shear velocity is also provided for comparison of the models.

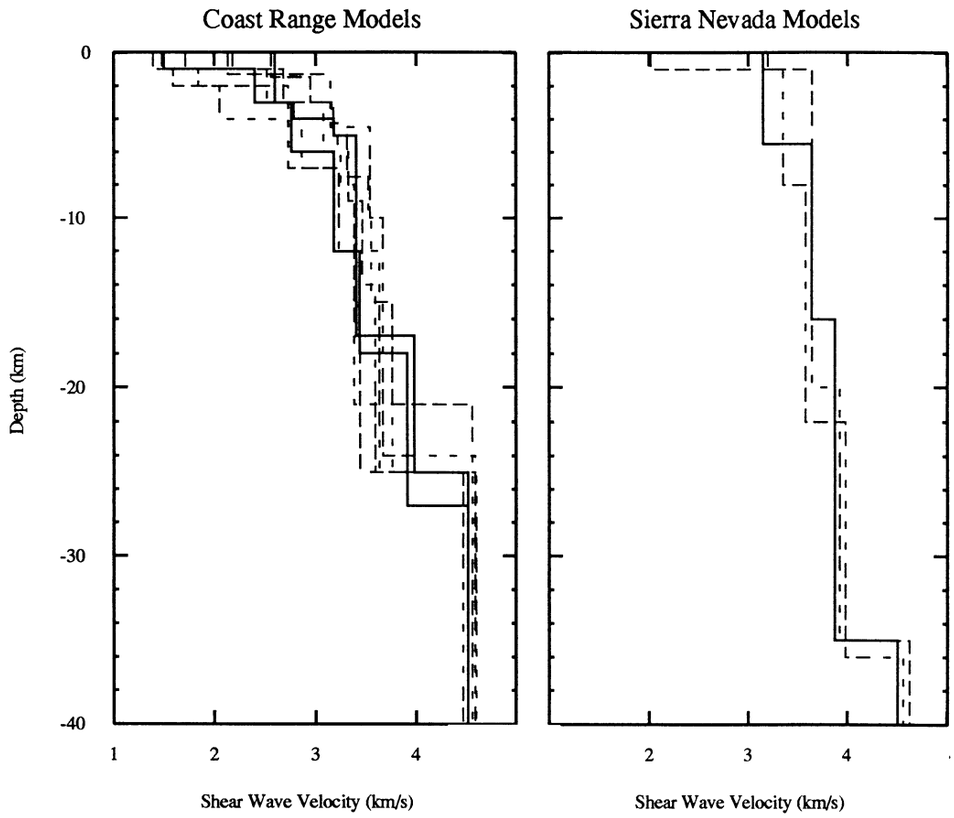

Figure 1. a) Central Coast Range S-wave velocity models derived from USGS P-wave models assuming a Poisson's ratio of 0.25 (dashed), and from broadband modeling of waveform data (solid). b) Sierra Nevada S-wave velocity models derived from USGS P-wave models assuming a Poisson's ration of 0.25 (dashed), and from broadband modeling of waveform data (solid).

Selected Moment Tensor Solutions Since January 1, 1990

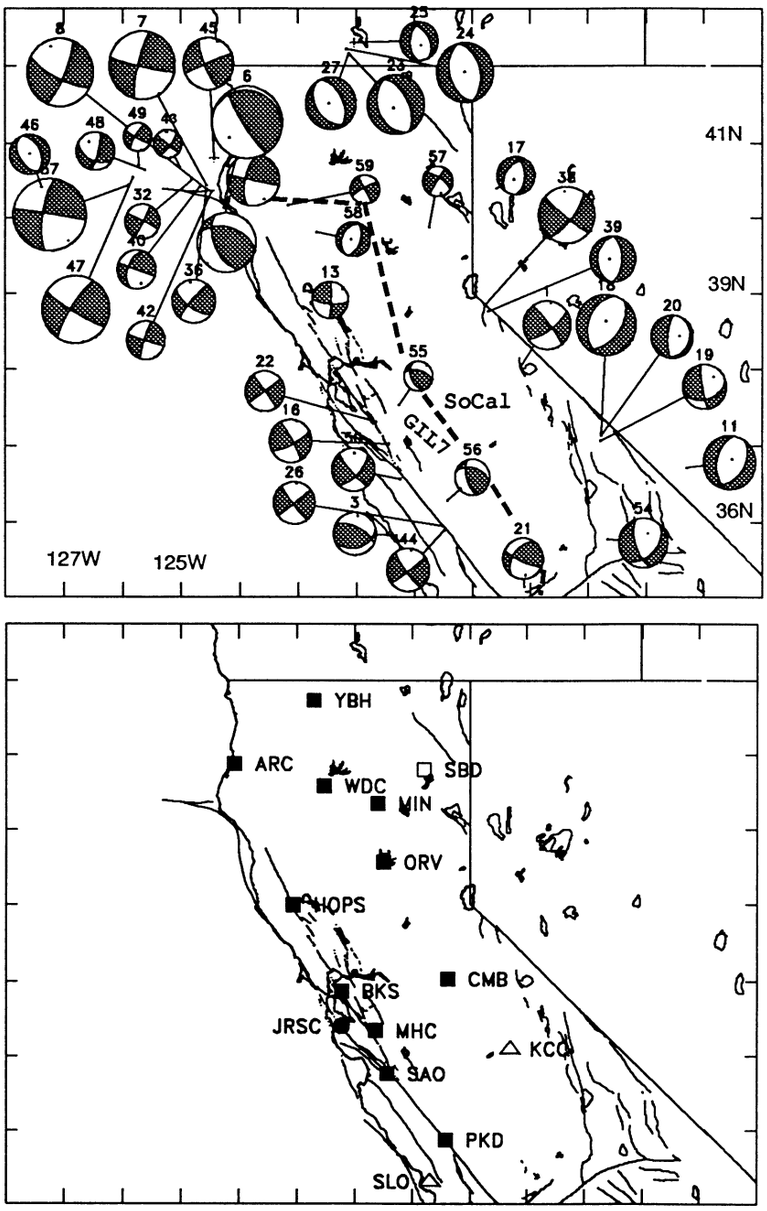

Figure 2. a) Moment tensor solutions for events since January 1990. The moment tensors were determined by inversion of complete, three-component low frequency (f<0.10Hz) waveform data recorded by BDSN. The events range in size from M_w 4.0 (evt 59) to M_w 6.9 (evt 37). b) Shows the configuration of the BDSN network.

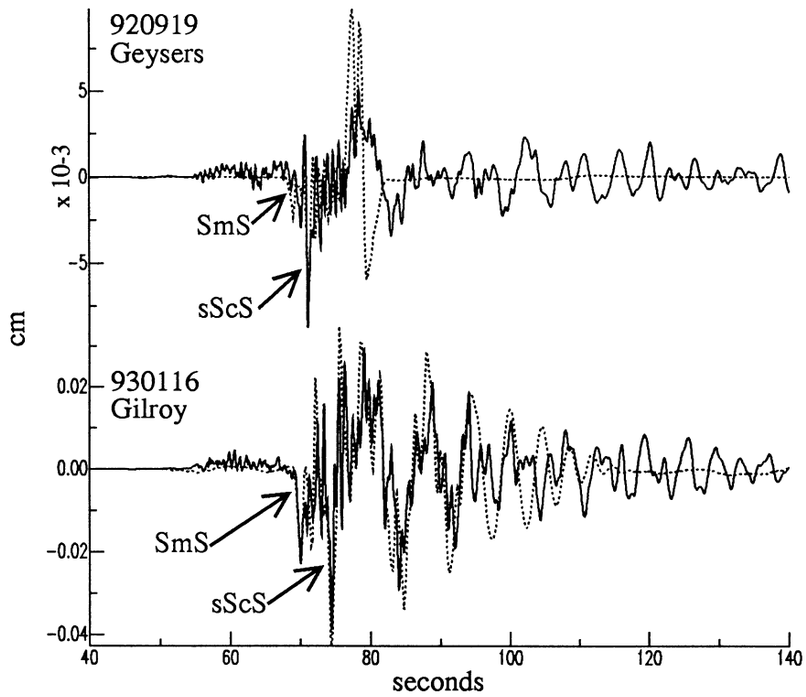

Figure 3. Compares tangential displacement data (0.02 to 2.0 Hz) for the Geysers and the Gilroy earthquakes (solid) with synthetics (dashed) computed with models MTM and GIL7 respectively. The critically reflected Moho reflection (SmS) and a depth phase reflecting off a mid-crustal interface at approximately 15 km depth (sScS) are labeled.

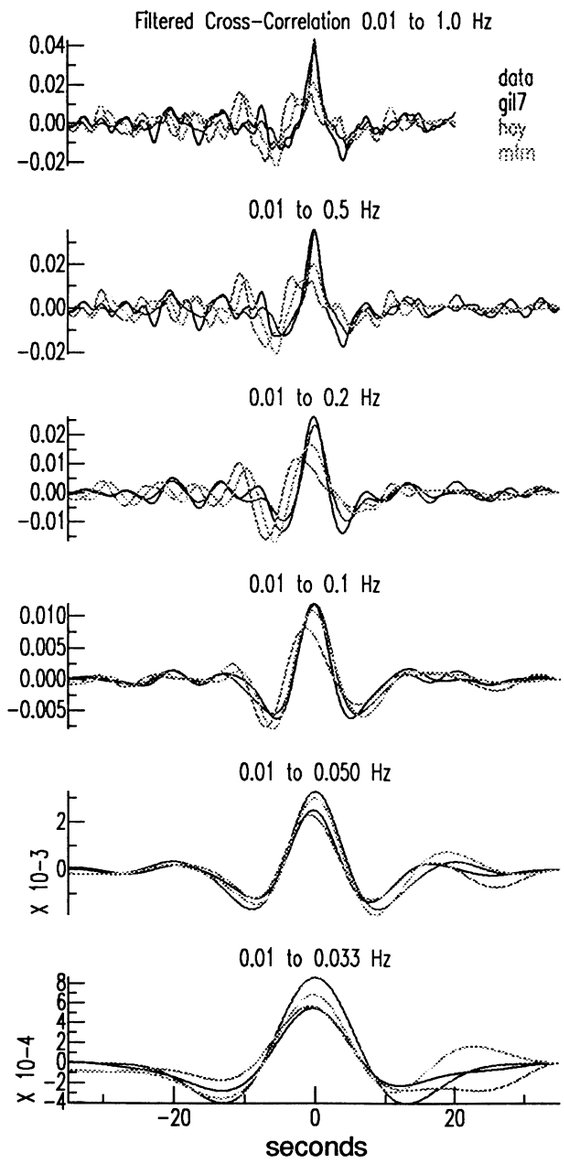

Figure 4. Bandpass filtered cross-correlagrams. The cross-correlagrams were formed by the cross-correlation of the tangential Gilroy data (Figure 3) with synthetics computed with models GIL7, HAY and MTM (Table 1). Note that the GIL7 cross-correlagram closely tracks the auto-correlation of the data in all of the frequency bands, and that at low frequencies (f<0.10 Hz) all of the models fit the data reasonably well.

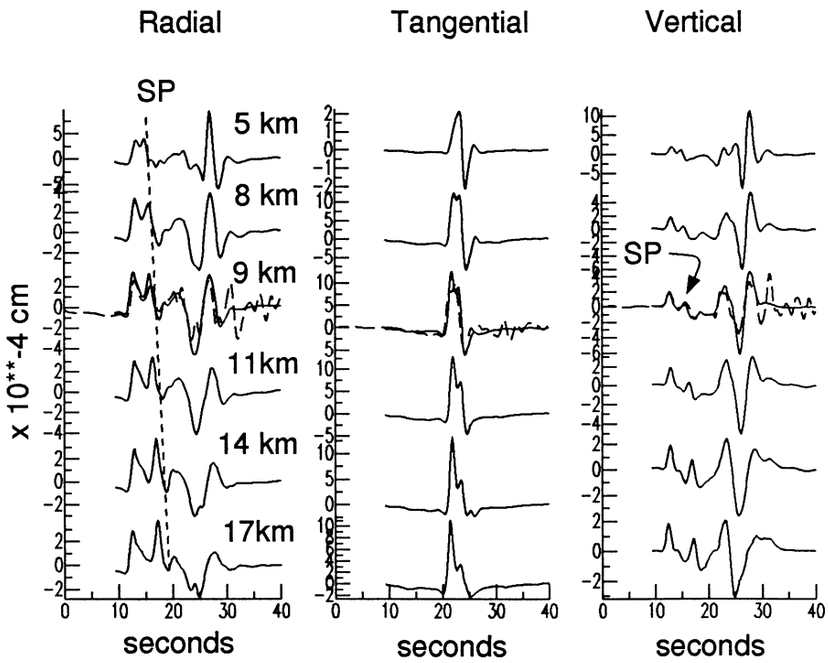

Figure 5. Comparison of three-component broadband (0.02 0.5 Hz) data (dashed) for a M_w 4.1 event located 71 km ENE of the ORV station (event 57 Figure 2) with synthetics (solid) computed with the SoCal model (Table 1). These seismograms are aligned in absolute traveltime and are well modeled by the synthetics computed for a depth of 9 km. Note that the free surface defraction SP is a strong arrival in the data and very important in providing source depth information.

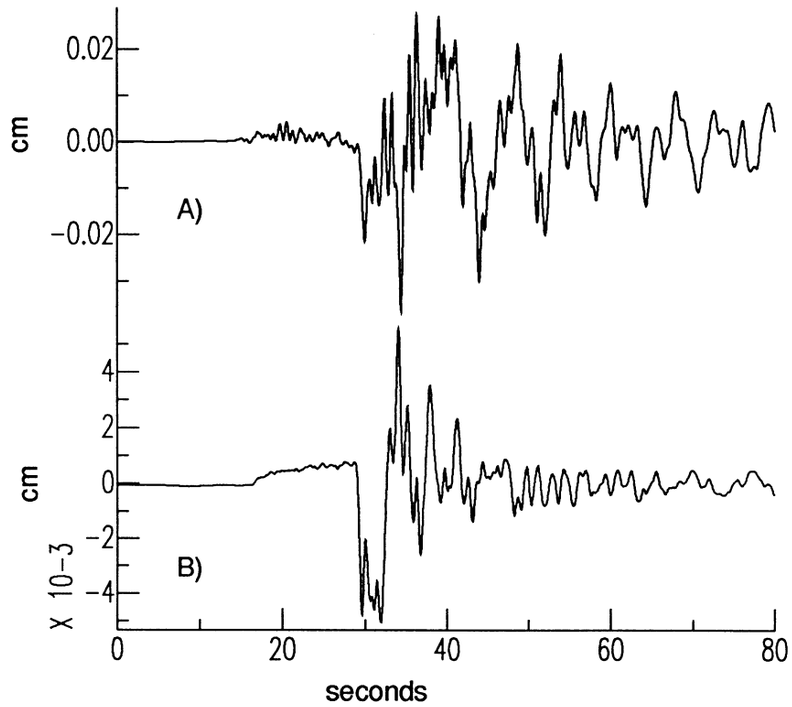

Figure 6. Comparison of a) the tangential BKS displacement record of the Gilroy earthquake, and b) the tangential CMB displacement record of a Double springs flat aftershock located near event 38 (Figure 2). This figure is intended to illustrate the substantial difference in waveform, particularly the dispersion of the Love waves, in the two velocity model domains.

Example of Automated Moment Tensor Determination
Mw3.9 Event 13 of SSW of Hollister, CA

Automatic Solution

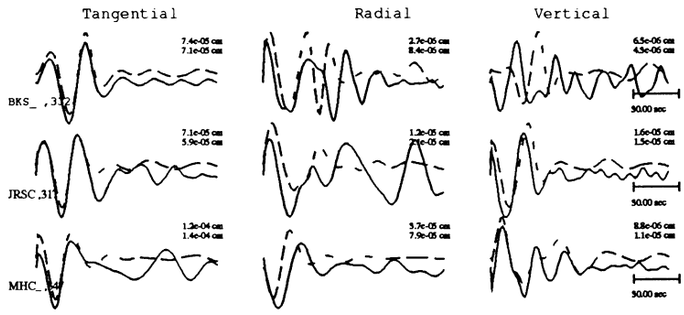

Strike=337 ; 73
Rake =154 ; 14
Dip =77 ; 65
Mo =8.85e+21
Mw =3.9
Percent DC=68
Percent CLVD=32
Variance=1.89e-10
Var. Red=5.91e+01
RES/Pdc.=2.77e-12

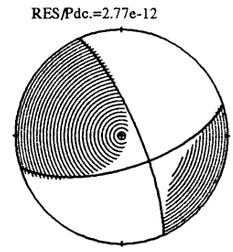

Final Solution

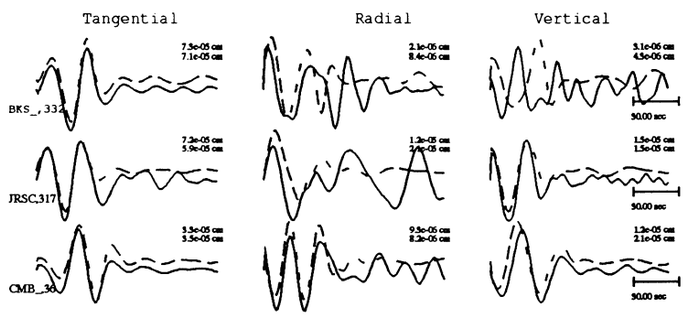

Strike=246 ; 336
Rake =-7 ; -177
Dip =87 ; 83
Mo =7.59e+21
Mw =3.9
Percent DC=93
Percent CLVD=7
Variance=2.84e-11
Var. Red=8.33e+01
RES/Pdc.=3.07e-13

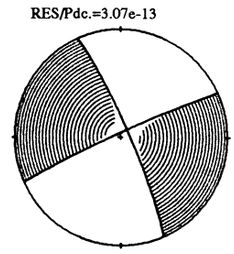

Event Chronology

OT 9506160420:36.5 UTC		
	0427:40	Event location Email received
	0429:34	Automatic MT solution
	0453	Final solution Emailed

Figure 7. Example of automated moment tensor solution for a M_w 3.9 earthquake. The automatic solution is very similar to the final result after analyst review. In this particular case the automatic solution was completed within 9 minutes of the event origin time.

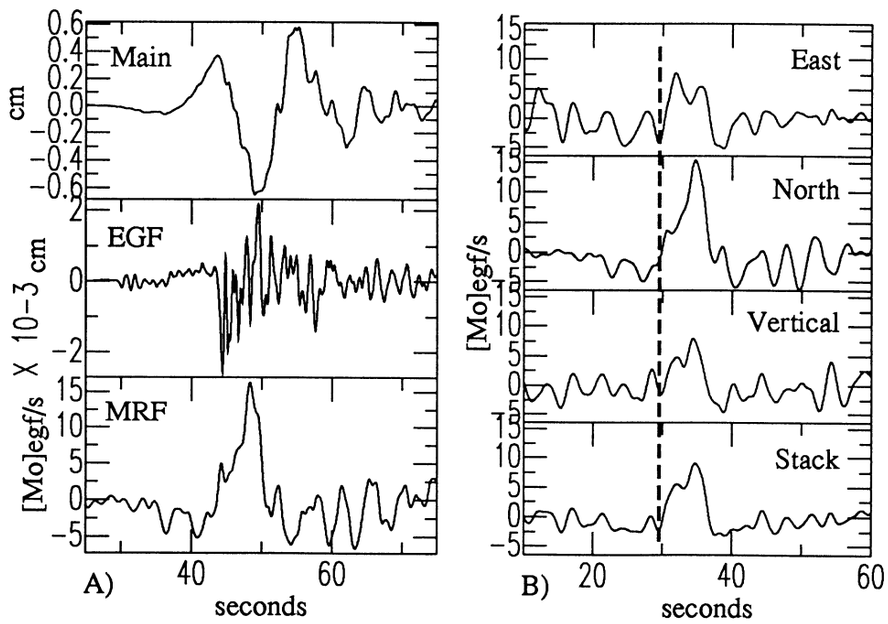

Figure 8. a) Example of empirical Green's function deconvolution. The trace labeled EGF was deconvolved from the trace labeled MAIN resulting in the far-field moment rate function (MRF). b) Far-field moment rate functions obtained be deconvolving each of the three components independently. The MRF in the lower right corner is the stack of the three-component deconvolutions and demonstrates the reduction of noise and emphasis of robust features provided by stacking. The dashed line marks the onset time of the MRF. The seismic moment of the EGF is $5.0x10^{22}$ dyne cm.

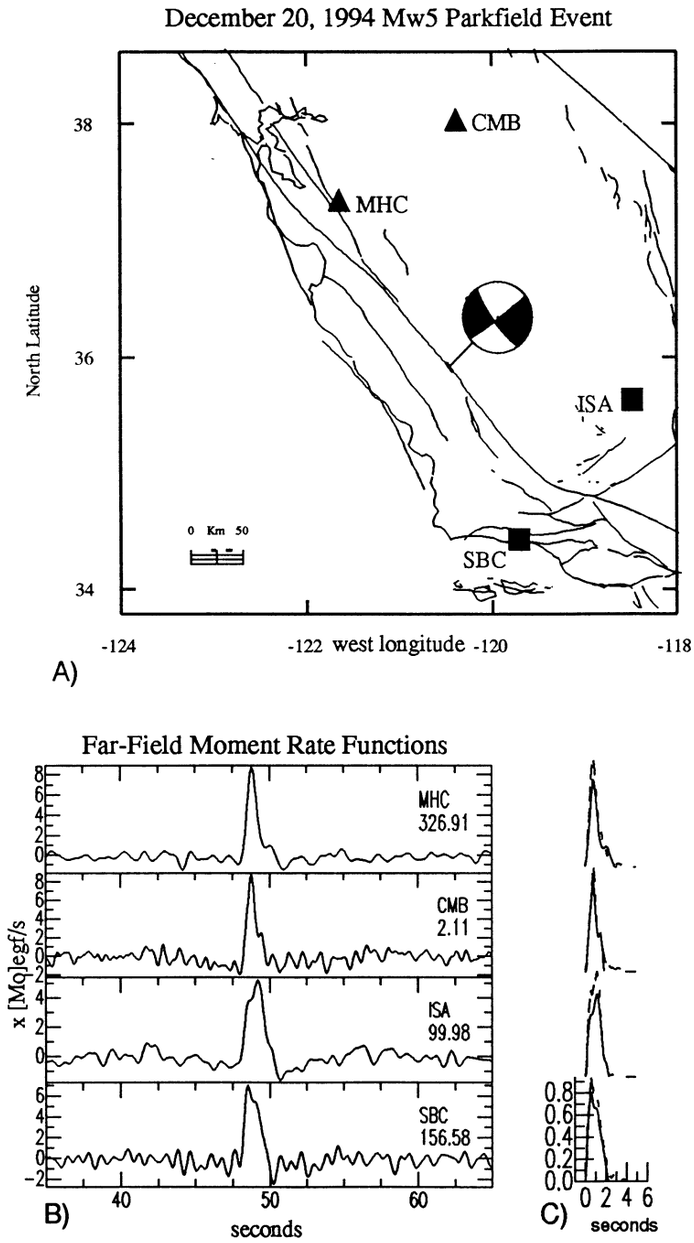

Figure 9. a) Map showing the location of four regional distance stations and the position of the December 20, 1994 M_w 5.0 Parkfield event. The moment tensor solution was obtained be inverting the long-period waveforms recorded at the four stations. b) Far-field moment rate functions obtained by deconvolving the motions of a smaller, nearby earthquake which occurred on October 20, 1992. The seismic moment of the EGF is $4.8x10^{22}$ dyne cm. c) Compares the MRF (solid) with synthetics (dashed). The pulses have been normalized to unit area.

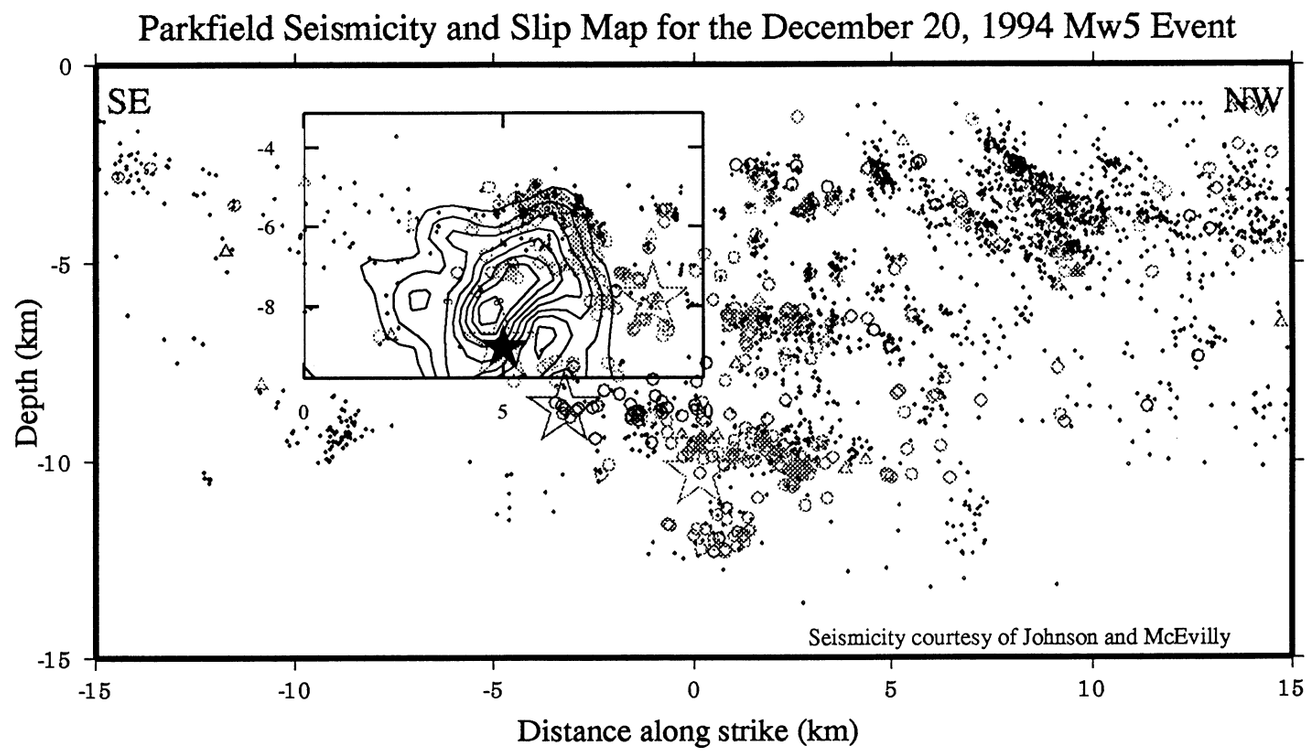

Figure 10. Slip map plotted over background Parkfield seismicity. The Parkfield background seismicity was obtained from Johnson and McEvilly. The light circles show events following the occurrence of the M_w 5.0 event. The slip tends to locate in a region which was devoid of background seismicity, and is bounded by clusters of events.

Appendix

I. Paper discussing implementation of various moment tensor methods at UC Berkeley (Romanowicz, B., D. Dreger, M. Pasyanos, and R. Uhrhammer, Monitoring of Strain Release in Central and Northern California Using Broadband Data, *Geophys. Res. Lett., 20,* 1643-1646, 1993, copyright by the American Geophysical Union).

II. Paper discussing the rupture process of the 1994 Northridge, CA earthquake using an empirical Green's function method (Dreger, D., Empirical Green's Function Study of the January 17, 1994 Northridge, California Earthquake, *Geophys. Res. Lett., 21,* 2633-2636, 1994, copyright by the American Geophysical Union).

III. Paper discussing the source process of the 1993 Klamath Falls, OR sequence (Dreger, D., J. Ritsema, and M. Pasyanos, Broadband Analysis of the 21 September, 1993, Klamath Falls Sequence, *Geophys. Res. Lett.,* 22, 997-1000, 1995, copyright by the American Geophysical Union).